**Computational Geosciences manuscript No.**
(will be inserted by the editor)

# A Cell-Centered Finite Difference Method for a Degenerate Elliptic Equation Arising from Two-Phase Mixtures

**Todd Arbogast · Abraham L. Taicher**

December 27, 2016 (revised)

**Abstract** We consider the linear degenerate elliptic system of two first order equations $\mathbf{u} = -d(\phi)^2(\nabla p - \mathbf{g})$ and $\nabla \cdot \mathbf{u} + \phi p = \phi^{1/2} f$, where $d$ satisfies $d(0) = 0$ and is otherwise positive, and the *porosity* $\phi \geq 0$ may be zero on a set of positive measure. This model equation has a similar degeneracy to that arising in the equations describing the mechanical system modeling the dynamics of partially melted materials, e.g., in the Earth's mantle and in polar ice sheets and glaciers. In the context of mixture theory, $\phi$ represents the phase variable separating the solid one-phase ($\phi = 0$) and fluid-solid two phase ($\phi > 0$) regions. After an appropriate scaling of the pressure and velocity, we obtain a well-posed mixed system, and we develop a cell-centered finite difference method based on lowest order Raviart-Thomas elements. The scheme is both stable and locally mass conservative. We present numerical results that show optimal rates of convergence and that superconvergence is attained for sufficiently regular solutions.

**Keywords** Degenerate elliptic, mixture theory, ice sheets, mantle dynamics, mixed method

**Mathematics Subject Classification (2000)** 65N12, 65N30, 35J70, 76M10, 76S05

## 1 Introduction

Flow in the Earth's mantle is modeled as a mixture of fluid melt and matrix solid [20, 1, 16, 15, 14, 2]. Both phases are assumed to exist at each point in the domain, and the porosity $\phi \geq 0$ represents the relative volume of the melted fluid to the bulk volume. This quantity is very small (a few percent) within the mantle. The

This work was supported by the U.S. National Science Foundation under grants EAR-1025321 and DMS-1418752.

Todd Arbogast · Abraham L. Taicher
The University of Texas at Austin, Institute for Computational Engineering and Sciences,
201 East 24th St. Stop C0200, Austin, TX 78712, USA
E-mail: arbogast@ices.utexas.edu, ataicher@gmail.com

matrix solid is deformable and modeled as a highly viscous Stokes fluid. Some of the solid may melt. If it does, it will do so between rock crystal boundaries [26], forming a porous medium, and so the interstitial fluid velocity $\mathbf{v}_\mathrm{f}$ is governed by Darcy's law.

Over the entire domain $\Omega \subset \mathbb{R}^n$, $n = 1$, 2, or 3, we have quantities for fluid (subscript f) and matrix solid (subscript s). These include the pressures $p_\mathrm{f}$ and $p_\mathrm{s}$, velocities $\mathbf{v}_\mathrm{f}$ and $\mathbf{v}_\mathrm{s}$, viscosities $\mu_\mathrm{f}$ and $\mu_\mathrm{s}$, and densities $\rho_\mathrm{f}$ and $\rho_\mathrm{s}$. Darcy's law takes the form

$$\phi(\mathbf{v}_\mathrm{f} - \mathbf{v}_\mathrm{s}) = -\frac{K(\phi)}{\mu_\mathrm{f}}(\nabla p_\mathrm{f} - \rho_\mathrm{f}\tilde{\mathbf{g}}), \tag{1}$$

for the permeability $K(\phi)$ and downward gravity vector $\tilde{\mathbf{g}}$. The fluid and solid stresses are

$$\boldsymbol{\sigma}_\mathrm{f} = -p_\mathrm{f}\mathbf{I} \quad \text{and} \quad \boldsymbol{\sigma}_\mathrm{s} = -p_\mathrm{s}\mathbf{I} + 2\mu_\mathrm{s}\big(\mathcal{D}\mathbf{v}_\mathrm{s} - \tfrac{1}{3}\nabla\cdot\mathbf{v}_\mathrm{s}\mathbf{I}\big),$$

where $\mathcal{D}\mathbf{v}_\mathrm{s} = \frac{1}{2}(\nabla\mathbf{v}_\mathrm{s} + \nabla\mathbf{v}_\mathrm{s}^T)$ is the symmetric gradient, and the mixture obeys the Stokes equation

$$\nabla\cdot\big(\phi\boldsymbol{\sigma}_\mathrm{f} + (1-\phi)\boldsymbol{\sigma}_\mathrm{s}\big) = \big(\phi\rho_\mathrm{f} + (1-\phi)\,\rho_\mathrm{s}\big)\tilde{\mathbf{g}}. \tag{2}$$

Conservation of mass, assuming constant and equal phase densities (or a Boussinesq approximation), gives the mixture equation

$$\nabla\cdot\big(\phi\mathbf{v}_\mathrm{f} + (1-\phi)\mathbf{v}_\mathrm{s}\big) = 0, \tag{3}$$

and a compaction relation is given as

$$\mu_\mathrm{s}\nabla\cdot\mathbf{v}_\mathrm{s} = \phi(p_\mathrm{f} - p_\mathrm{s}). \tag{4}$$

The system (1)–(4) describes the mechanics of flow. In addition to this system, the full problem requires equations describing the thermodynamics, phase behavior, and component mass equations to define the porosity $\phi$ itself. In this paper, we study only the mechanics of the flow; that is, we will assume that the porosity $\phi : \Omega \to [0, \phi^*]$, $0 < \phi^* < \infty$, is given as a differentiable function.

Because the Darcy and Stokes systems have been combined using mixture theory, we have a single, two-phase model that holds at every point of space even when the fluid phase disappears. The free boundary between the one and two phase regions need not be determined. Similar mixture models arise in modeling two-phase flow within a non-deformable porous medium [7,17,8,11] and in the modeling of partially melted ice, e.g., in glacier dynamics [13,6,24].

The system (1)–(4) is degenerate in $\phi$ in the absence of fluid melt. Since there is always matrix rock present at each point of space, the Stokes part is well-posed, (i.e., $\phi \le \phi^* < 1$). In this paper we will focus on the degenerate Darcy part of the system. In fact, we generalize this part of the system. In terms of a Darcy velocity $\mathbf{u} = \phi(\mathbf{v}_f - \mathbf{v}_\mathrm{s})$ and a pressure $p = p_\mathrm{f}$, we consider the linear degenerate elliptic boundary value problem

$$\mathbf{u} = -d(\phi)^2(\nabla p - \mathbf{g}) \quad \text{in } \Omega, \tag{5}$$

$$\nabla\cdot\mathbf{u} + \phi\, p = \phi^{1/2} f \quad \text{in } \Omega, \tag{6}$$

$$\mathbf{u}\cdot\boldsymbol{\nu} = \phi^{1/2} g_\mathrm{N} \quad \text{on } \Gamma_\mathrm{N}, \tag{7}$$

where $\Gamma_{\rm N} = \partial\Omega$, $\boldsymbol{\nu}$ is the outward unit normal vector and $g_{\rm N}$ is a given function. We assume that $d$ lies in $C^1([0,\phi^*])$ with $d(0) = 0$ and $d$ positive on $(0,\phi^*]$. To connect back to (1) and (4) minus $\mu_{\rm s}$ times (3), we would take $\mu_{\rm s} = 1$, $f = \phi^{1/2} p_{\rm s}$, $d(\phi) = \sqrt{K(\phi)/\mu_{\rm f}}$, and $\mathbf{g} = \rho_{\rm f}\tilde{\mathbf{g}}$. In place of the Neumann boundary condition (7), we could impose a Dirichlet or Robin boundary condition of the form

$$\phi p - \kappa^2 \mathbf{u}\cdot\boldsymbol{\nu} = \phi^{1/2} g_{\rm R} \quad \text{on } \Gamma_{\rm R}, \tag{8}$$

where now $\Gamma_{\rm N} = \emptyset$, $\Gamma_{\rm R} = \partial\Omega$, and $\kappa \geq 0$ and $g_{\rm R}$ are given functions. Moreover, we set $\Gamma_{\rm R} = \emptyset$ when $\Gamma_{\rm N} = \partial\Omega$.

Many works describe approximation of degenerate elliptic equations, e.g., [12, 19,5,18,9], using weighted Sobolev spaces and least squares techniques. But the degeneracies are always required to lie on a set of measure zero. It is important in this application that $\phi$ may vanish on a set of positive measure.

The system (5)–(6) with either (7) or (8) was studied in [3]. After a change of dependent variables, the system was shown to be well-posed under suitable hypotheses. Moreover, a mixed finite element method was defined and shown to be optimally convergent. In this paper, we will develop a cell-centered finite element method that is easier to implement, much easier to solve numerically, locally mass conservative, and exhibits better convergence behavior (i.e., superconvergence) in the numerical examples. The method will be applied to the simulation of the full set of mechanics equations of the mantle dynamics problem in [2] with Professor Marc A. Hesse.

In the rest of the paper, we recall the theory developed in [3] in the next section. We include a description of the scaled equations and scaled variational formulation of the problem. In Section 3, we define our cell-centered finite difference method, discuss implementation, and prove local mass conservation and stability. One and two dimensional numerical results are presented in Section 4, where we show that the scheme achieves superconvergence when the solution has sufficient regularity. We provide concluding remarks in the last section.

## 2 A scaled formulation and review of theoretical results

Let $(\cdot,\cdot)$ denote the $L^2(\Omega)$ inner-product or possibly duality pairing, and $\langle\cdot,\cdot\rangle$ denote the $L^2(\partial\Omega)$ inner-product or duality pairing. In fact, denote the latter form by $\langle\cdot,\cdot\rangle_{\rm N}$ or $\langle\cdot,\cdot\rangle_{\rm R}$ in the cases of Neumann or Robin boundary conditions, respectively, where the form is interpreted as zero in the contrary case. Let $\|\cdot\|_{r,p,S}$ denote the norm of the standard Sobolev space $W^{r,p}(S)$, wherein we omit $p$ if it is 2 and then also $r$ if it is 0, and we omit $S$ if it is $\Omega$. Recall that $H^r(S) = W^{r,2}(S)$.

Let the *scaled velocity* and *scaled pressure* be defined formally as

$$\mathbf{v} = d(\phi)^{-1}\mathbf{u}, \tag{9}$$

$$q = \phi^{1/2} p, \tag{10}$$

respectively. At least when $\phi > 0$, the system (5)–(8) becomes

$$\mathbf{v} = -d(\phi)\big(\nabla(\phi^{-1/2}q) - \mathbf{g}\big) \quad \text{in } \Omega, \tag{11}$$
$$\phi^{-1/2}\nabla\cdot(d(\phi)\mathbf{v}) + q = f \quad \text{in } \Omega, \tag{12}$$
$$d(\phi)\mathbf{v}\cdot\boldsymbol{\nu} = \phi^{1/2}g_{\mathrm{N}} \quad \text{on } \Gamma_{\mathrm{N}}, \tag{13}$$
$$q - \kappa^2\phi^{-1/2}d(\phi)\mathbf{v}\cdot\boldsymbol{\nu} = g_{\mathrm{R}} \quad \text{on } \Gamma_{\mathrm{R}}. \tag{14}$$

The mathematical structure of this system is easily seen if one defines the operator $A = \phi^{-1/2}\nabla\cdot(d(\phi)(\cdot))$. Neglecting terms coming from the boundary conditions, the formal adjoint of $A$ is $A^* = -d(\phi)\nabla(\phi^{-1/2}(\cdot))$. Thus (11)–(12) is

$$\begin{aligned} \mathbf{v} - A^*q &= d(\phi)\mathbf{g} \quad \text{in } \Omega, \\ A\mathbf{v} + q &= f \quad \text{in } \Omega, \end{aligned}$$

and so the operator of the system is the sum of the identity and an antisymmetric operator.

## 2.1 The space $H_{\phi,d}(\mathrm{div})$

To ensure that the differential operators in (11)–(12) make sense, we note that

$$\phi^{-1/2}\nabla\cdot(d(\phi)\mathbf{v}) = \phi^{-1/2}\nabla d(\phi)\cdot\mathbf{v} + \phi^{-1/2}d(\phi)\nabla\cdot\mathbf{v}, \tag{15}$$
$$d(\phi)\nabla(\phi^{-1/2}q) = -\tfrac{1}{2}\phi^{-3/2}d(\phi)\nabla\phi\, q + \phi^{-1/2}d(\phi)\nabla q. \tag{16}$$

We therefore make the following assumption on $\phi$.

**Assumption 1** *The function $\phi : \Omega \to [0,\phi^*]$, $0 < \phi^* < \infty$, is differentiable and satisfies*

1. $\phi^{-1/2}\nabla d(\phi) \in (L^\infty(\Omega))^n$,
2. $\phi^{-1/2}d(\phi) \in L^\infty(\Omega)$,
3. $\phi^{-3/2}d(\phi)\nabla\phi \in (L^\infty(\Omega))^n$.

Since in (16), we take $q \in H^1(\Omega)$ and require the resulting function to be in $(L^2(\Omega))^n$, we can relax point 3 using the Sobolev Embedding Theorem to require only that

$$\phi^{-3/2}d(\phi)\nabla\phi \in \begin{cases} (L^2(\Omega))^n & \text{if } n = 1, \\ (L^{2+\epsilon}(\Omega))^n & \text{if } n = 2 \text{ (any } \epsilon > 0), \\ (L^n(\Omega))^n & \text{if } n \geq 3. \end{cases}$$

As in [3], we can now define the space

$$H_{\phi,d}(\mathrm{div};\Omega) = \big\{\mathbf{v} \in (L^2(\Omega))^n \,:\, \phi^{-1/2}\nabla\cdot(d(\phi)\mathbf{v}) \in L^2(\Omega)\big\}. \tag{17}$$

This space admits a normal trace operator $\gamma_{\phi,d} : H_{\phi,d}(\mathrm{div};\Omega) \to H^{-1/2}(\partial\Omega)$ for $w \in H^{1/2}(\partial\Omega)$ extended to $w \in H^1(\Omega)$ defined by the integration by parts formula

$$\langle\gamma_{\phi,d}(\mathbf{v}), w\rangle = \big(\phi^{-1/2}\nabla\cdot(d(\phi)\mathbf{v}), w\big) + \big(\mathbf{v}, d(\phi)\nabla(\phi^{-1/2}w)\big). \tag{18}$$

We can interpret $\gamma_{\phi,d}(\mathbf{v}) = \phi^{-1/2} d(\phi)\mathbf{v}\cdot\boldsymbol{\nu}$. Finally, we can apply the homogeneous Neumann boundary condition to define the space

$$H_{\phi,d,0}(\mathrm{div};\Omega) = \big\{\mathbf{v} \in H_{\phi,d}(\mathrm{div};\Omega) \ : \ \gamma_{\phi,d}(\mathbf{v}) = \phi^{-1/2} d(\phi)\mathbf{v}\cdot\boldsymbol{\nu} = 0 \text{ on } \partial\Omega\big\}, \quad (19)$$

and we can define the image space of the normal trace operator by

$$H_{\phi,d}^{-1/2}(\partial\Omega) = \gamma_{\phi,d}\big(H_{\phi,d}(\mathrm{div};\Omega)\big) \subset H^{-1/2}(\partial\Omega). \quad (20)$$

The following result is proved in [3].

**Lemma 1** *If Assumption 1 holds, then $H_{\phi,d}(\mathrm{div};\Omega)$ is a Hilbert space with the inner-product*

$$(\mathbf{u},\mathbf{v})_{H_{\phi,d}(\mathrm{div})} = (\mathbf{u},\mathbf{v}) + \big(\phi^{-1/2}\nabla\cdot(d(\phi)\mathbf{u}), \phi^{-1/2}\nabla\cdot(d(\phi)\mathbf{v})\big). \quad (21)$$

*Moreover, the normal trace operator $\gamma_{\phi,d} : H_{\phi,d}(\mathrm{div};\Omega) \to H^{-1/2}(\partial\Omega)$ is well defined by* (18)*, and there is a constant $C > 0$ such that*

$$\|\gamma_{\phi,d}(\mathbf{v})\|_{-1/2,\partial\Omega} = \|\phi^{-1/2} d(\phi)\mathbf{v}\cdot\boldsymbol{\nu}\|_{-1/2,\partial\Omega} \le C\|\mathbf{v}\|_{H_{\phi,d}(\mathrm{div};\Omega)} \quad (22)$$

*for any $\mathbf{v} \in H_{\phi,d}(\mathrm{div};\Omega)$.*

We remark in passing that $H(\mathrm{div};\Omega) = \big\{\mathbf{v} \in (L^2(\Omega))^n \ : \ \nabla\cdot\mathbf{v} \in L^2(\Omega)\big\} \subset H_{\phi,d}(\mathrm{div};\Omega)$ for any admissible $\phi$ and $d$.

## 2.2 A scaled weak formulation and unique existence of the solution

To unify the treatment of boundary conditions, let $\mathbf{V}$ be $H_{\phi,d,0}(\mathrm{div};\Omega)$ when $\Gamma_{\mathrm{N}} = \partial\Omega$ and let $\mathbf{V}$ be $H_{\phi,d}(\mathrm{div};\Omega)$ when $\Gamma_{\mathrm{R}} = \partial\Omega$. In the case of Neumann boundary conditions, suppose that $g_{\mathrm{N}} \in H_{\phi,d}^{-1/2}(\partial\Omega)$. Then there is some $\mathbf{v}_{\mathrm{N}} \in H_{\phi,d}(\mathrm{div};\Omega)$ such that

$$\gamma_{\phi,d}(\mathbf{v}_{\mathrm{N}}) = \phi^{-1/2} d(\phi)\mathbf{v}_{\mathrm{N}}\cdot\boldsymbol{\nu} = g_{\mathrm{N}}. \quad (23)$$

When using Robin conditions, let $\mathbf{v}_{\mathrm{N}} = 0$.

The weak formulation of (11)–(14) is: Find $\mathbf{v} \in \mathbf{V} + \mathbf{v}_{\mathrm{N}}$ and $q \in L^2(\Omega)$ such that

$$\begin{aligned} &(\mathbf{v},\boldsymbol{\psi}) - \big(q, \phi^{-1/2}\nabla\cdot(d(\phi)\boldsymbol{\psi})\big) + \langle\kappa^2\phi^{-1}(d(\phi))^2\mathbf{v}\cdot\boldsymbol{\nu}, \boldsymbol{\psi}\cdot\boldsymbol{\nu}\rangle_{\mathrm{R}} \quad (24)\\ &\quad = (d(\phi)\mathbf{g},\boldsymbol{\psi}) - \langle g_{\mathrm{R}}, \phi^{-1/2} d(\phi)\boldsymbol{\psi}\cdot\boldsymbol{\nu}\rangle_{\mathrm{R}} \qquad \forall\boldsymbol{\psi} \in \mathbf{V},\\ &\big(\phi^{-1/2}\nabla\cdot(d(\phi)\mathbf{v}), w\big) + (q,w) = (f,w) \qquad \forall w \in L^2(\Omega). \quad (25)\end{aligned}$$

The following result is proved in [3].

**Theorem 1** *Let Assumption 1 hold, $f \in L^2(\Omega)$, and $d(\phi)\mathbf{g} \in (L^2(\Omega))^n$. If $\Gamma_{\mathrm{N}} = \partial\Omega$, let $g_{\mathrm{N}} \in H_{\phi,d}^{-1/2}(\partial\Omega)$ and $\mathbf{v}_{\mathrm{N}} \in H_{\phi,d}(\mathrm{div};\Omega)$ be defined by* (23)*, and if $\Gamma_{\mathrm{R}} = \partial\Omega$, let $g_{\mathrm{R}} \in H^{1/2}(\partial\Omega)$ and $\mathbf{v}_{\mathrm{N}} = 0$. Then there is a unique solution to the problem* (24)–(25)*, and the following energy estimates hold:*

$$\begin{aligned} &\|\mathbf{v}\| + \|q\| + \|\phi^{-1/2}\nabla\cdot(d(\phi)\mathbf{v})\| + \|\kappa\phi^{-1/2} d(\phi)\mathbf{v}\cdot\boldsymbol{\nu}\|_{0,\Gamma_{\mathrm{R}}} \quad (26)\\ &\quad \le C\big\{\|f\| + \|d(\phi)\mathbf{g}\| + \|\mathbf{v}_{\mathrm{N}}\| + \|\phi^{-1/2}\nabla\cdot(d(\phi)\mathbf{v}_{\mathrm{N}})\| + \|g_{\mathrm{R}}\|_{1/2,\Gamma_{\mathrm{R}}}\big\}.\end{aligned}$$

The system (24)–(25) is equivalent to our original system (5)–(8) on the support of $\phi$, but it remains well posed wherever $\phi = 0$. Assumption 1 appears to be necessary for the variational formulation to be well-defined. It is unclear if this assumption holds for the full mantle dynamics problem. As noted after (4), there are several additional equations needed to describe the dynamics of $\phi$ itself. There is currently no existence and uniqueness result for this larger system, much less a theory of the regularity of $\phi$.

## 3 A cell-centered finite difference method based on $\mathbf{RT_0}$

We now give our discrete version of the scaled system (24)–(25). We assume that $\Omega$ is a rectangle ($n = 2$) or brick ($n = 3$), and impose a rectangular finite element mesh $\mathcal{T}_h$ over the domain of maximal spacing $h$. Let $\mathcal{E}_h$ denote the set of element edges ($n = 2$) or faces ($n = 3$). We use the notation $|E|$ for the measure (area or volume) of $E \in \mathcal{T}_h$ and $|e|$ for the measure (length or area) of $e \in \mathcal{E}_h$. Let $\mathbb{P}_r$ be the set of polynomials of total degree $r$ and let $\mathbb{P}_{r_1,r_2,r_3}$ (omit $r_3$ if $n = 2$) be the set of polynomials of degree $r_i$ in $x_i$ for each $i = 1, \ldots, n$.

To develop our cell-centered finite difference method, we relate it to the lowest order Raviart-Thomas ($\mathrm{RT}_0$) finite element space $\mathbf{V}_h^{\mathrm{full}} \times W_h$ [21,10,22]. On an element $E \in \mathcal{T}_h$, $\mathbf{V}_h(E) = \mathbb{P}_{1,0,0} \times \mathbb{P}_{0,1,0} \times \mathbb{P}_{0,0,1}$ (omit the last component if $n = 2$) and $W_h(E) = \mathbb{P}_0$. To handle the boundary condition, define the space $\mathbf{V}_h^0 = \{\mathbf{v}_h \in \mathbf{V}_h^{\mathrm{full}} : \mathbf{v}_h \cdot \boldsymbol{\nu} = 0 \text{ on } \partial\Omega\}$, and finally let $\mathbf{V}_h$ be $\mathbf{V}_h^0$ when $\Gamma_{\mathrm{N}} = \partial\Omega$ and $\mathbf{V}_h^{\mathrm{full}}$ when $\Gamma_{\mathrm{R}} = \partial\Omega$.

We will make use of the usual projection operators associated with $\mathrm{RT}_0$. Let $\mathcal{P}_{W_h} = \hat{\cdot} : L^2(\Omega) \to W_h$ denote the $L^2(\Omega)$ projection operator, which projects a function into the space of piecewise constant functions. Moreover, let $\pi : H(\mathrm{div};\Omega) \cap L^{2+\epsilon}(\Omega) \to \mathbf{V}_h$ (any $\epsilon > 0$) denote the standard Raviart-Thomas or Fortin operator [21,22] that preserves element average divergence and edge normal fluxes [10, Section III.3.3].

### 3.1 The method

Denote the local average of $\phi$ over element $E \in \mathcal{T}_h$ by

$$\phi_E = \frac{1}{|E|} \int_E \phi \, dx = \hat{\phi}|_E. \tag{27}$$

Let the trapezoidal quadrature rule be denoted by $(\cdot,\cdot)_Q$ , i.e., if $x_{E,j}$ denotes a vertex of element $E \in \mathcal{T}_h$, then

$$(\mathbf{v}_h, \boldsymbol{\psi})_Q = \sum_{E \in \mathcal{T}_h} \frac{|E|}{2^n} \sum_{j=1}^{2^n} \mathbf{v}_h(x_{E,j}) \cdot \boldsymbol{\psi}(x_{E,j}). \tag{28}$$

In variational form, our method is: Find $\mathbf{v}_h \in \mathbf{V}_h + \mathbf{v}_{\mathrm{N}}$ and $q_h \in W_h$ such that

$$\begin{aligned} &(\mathbf{v}_h, \boldsymbol{\psi})_Q - \big(q_h, \hat{\phi}^{-1/2} \nabla \cdot (d(\phi)\boldsymbol{\psi})\big) + \langle \kappa^2 \phi^{-1} (d(\phi))^2 \mathbf{v}_h \cdot \boldsymbol{\nu}, \boldsymbol{\psi} \cdot \boldsymbol{\nu} \rangle_{\mathrm{R}} \qquad (29)\\ &\quad = (d(\phi)\mathbf{g}, \boldsymbol{\psi}) - \langle g_{\mathrm{R}}, \phi^{-1/2} d(\phi) \boldsymbol{\psi} \cdot \boldsymbol{\nu} \rangle_{\mathrm{R}} \qquad \forall \boldsymbol{\psi} \in \mathbf{V}_h,\\ &\big(\hat{\phi}^{-1/2} \nabla \cdot (d(\phi)\mathbf{v}_h), w\big) + (q_h, w) = (\hat{\phi}^{-1/2} \phi^{1/2} f, w) \qquad \forall w \in W_h, \qquad (30) \end{aligned}$$

with the convention that on an element $E$ when $\hat{\phi}|_E = \phi_E = 0$, we set the divergence terms to zero, and in that case, $\hat{\phi}^{-1/2}\phi^{1/2} f = f$. The use of quadrature and the replacement of $\phi$ by $\hat{\phi}$ allows us to reformulate the method as a cell-centered finite difference method [23,4], as we will see below.

We easily recover the discrete pressure $p_h \in W_h$ by setting for all $E \in \mathcal{T}_h$

$$p_h|_E = \begin{cases} 0 & \text{if } \phi_E = 0, \\ \phi_E^{-1/2} q_h|_E & \text{if } \phi_E \neq 0, \end{cases} \tag{31}$$

where we have arbitrarily set $p_h|_E$ to zero when $\phi_E = 0$, since it is otherwise ill-defined. The discrete velocity $\mathbf{u}_h \in \mathbf{V}_h + \mathbf{v}_\mathrm{N}$ is defined by setting for all $e \in \mathcal{E}_h$

$$\mathbf{u}_h \cdot \boldsymbol{\nu}|_e = \frac{1}{|e|} \int_e d(\phi)\, ds\, \mathbf{v}_h \cdot \boldsymbol{\nu}|_e, \tag{32}$$

so that $\pi \mathbf{u}_h = \pi(d(\phi)\mathbf{v}_h)$.

### 3.2 Implementation

We now discuss in detail implementation of the method. The degrees of freedom for $\mathbf{V}_h$ are the constant normal values on the edges or faces, and the degrees of freedom of $W_h$ are the average values over the elements. Let bases be defined, respectively, by

$$\left\{\mathbf{v}_e \,:\, \mathbf{v}_e \cdot \boldsymbol{\nu}|_f = \delta_{e,f} \;\forall e, f \in \mathcal{E}_h\right\} \text{ and } \left\{w_E \,:\, w_E|_F = \delta_{E,F} \;\forall E, F \in \mathcal{T}_h\right\},$$

where $\delta_{i,j}$ is the Kronecker delta function for indices $i$ and $j$. (In the case of Neumann boundary conditions, we omit the basis functions with degrees of freedom supported on $\Gamma_\mathrm{N} = \partial\Omega$.)

In this basis, the linear system corresponding to the method (29)–(30) is

$$\begin{pmatrix} A & -B \\ B^T & C \end{pmatrix} \begin{pmatrix} v \\ q \end{pmatrix} = \begin{pmatrix} a \\ b \end{pmatrix}, \tag{33}$$

wherein $v$ and $q$ represent the degrees of freedom for $\mathbf{v}$ and $q$, respectively. Because of the quadrature rule, it is easy to compute

$$\begin{aligned} A_{e,f} &= (\mathbf{v}_e, \mathbf{v}_f)_Q + \langle \kappa^2 \phi^{-1} (d(\phi))^2 \mathbf{v}_e \cdot \boldsymbol{\nu}, \mathbf{v}_f \cdot \boldsymbol{\nu} \rangle_\mathrm{R} \qquad (34) \\ &= \Big(\frac{1}{2}|E_e| + \int_{e \cap \Gamma_\mathrm{R}} \kappa^2 \phi^{-1} (d(\phi))^2\, ds\Big) \delta_{e,f}, \\ C_{E,F} &= (w_E, w_F) = |E|\, \delta_{E,F}, \qquad (35) \end{aligned}$$

where $E_e$ is the support of $\mathbf{v}_e$ (i.e., the one or two elements adjacent to $e$). Moreover,

$$\begin{aligned} a_e &= (d(\phi)\mathbf{g}, \mathbf{v}_e) - \langle g_\mathrm{R}, \phi^{-1/2} d(\phi) \mathbf{v}_e \cdot \boldsymbol{\nu} \rangle_\mathrm{R} \qquad (36) \\ &= \int_{E_e} d(\phi)\mathbf{g} \cdot \mathbf{v}_e\, dx - \mathbf{v}_e \cdot \boldsymbol{\nu} \int_{e \cap \Gamma_\mathrm{R}} g_\mathrm{R} \phi^{-1/2} d(\phi)\, ds, \\ b_E &= (\hat{\phi}^{-1/2}\phi^{1/2} f, w_E) = \begin{cases} \displaystyle\int_E f\, dx & \text{if } \phi_E = 0, \\ \displaystyle\phi_E^{-1/2} \int_E \phi^{1/2} f\, dx & \text{if } \phi_E \neq 0. \end{cases} \qquad (37) \end{aligned}$$

The matrix $B$ remains, but it is clear how it is defined because we have avoided division by $\phi$ when $\phi = 0$. It is

$$B_{e,E} = \big(\hat{\phi}^{-1/2}\nabla\cdot(d(\phi)\mathbf{v}_e), w_E\big) = \langle \phi_E^{-1/2} d(\phi)\mathbf{v}_e\cdot\boldsymbol{\nu}, w_E\rangle_{\partial E};$$

that is,

$$B_{e,E} = \begin{cases} 0 & \text{if } e \not\subset \partial E \text{ or } \phi_E = 0, \\ \phi_E^{-1/2}\mathbf{v}_e\cdot\boldsymbol{\nu}_E \displaystyle\int_e d(\phi)\,dx & \text{if } e \subset \partial E \text{ and } \phi_E \neq 0. \end{cases} \tag{38}$$

The Schur complement of (33) for $q$ is

$$v = A^{-1}(Bq + a), \tag{39}$$

$$(B^T A^{-1} B + C)\, q = b - B^T A^{-1} a. \tag{40}$$

The matrix of the second equation can be formed easily as a 5- or 7-point finite difference stencil for $n = 2$ or 3, respectively, because $A$ is diagonal and positive definite [23,4]. Thus we solve the second equation (40) relatively efficiently as a cell-centered finite difference method for $q$, and then form $v$ using $q$ and the first equation (39).

### 3.3 Local mass conservation

**Lemma 2** *The finite element method* (29)–(30) *conserves mass locally over each element of the computational mesh, that is,*

$$\int_E \nabla\cdot\mathbf{u}_h\,dx + \int_E \phi\, p_h\,dx = \int_E \phi^{1/2} f\,dx \quad \textit{for all } E \in \mathcal{T}_h, \tag{41}$$

*which is the mass conservation equation* (6) *integrated over* $E$.

*Proof* In fact, the equation (30) alone implies that mass is conserved locally by the method. We simply take the test function $\phi_E^{1/2} w_E \in W_h$ to see that

$$\int_E \nabla\cdot(d(\phi)\mathbf{v}_h)\,dx + \int_E \phi_E^{1/2} q_h\,dx = \int_E \phi^{1/2} f\,dx, \tag{42}$$

which is the same as

$$\int_E \nabla\cdot\pi(d(\phi)\mathbf{v}_h)\,dx + \int_E \phi\,\phi_E^{-1/2} q_h\,dx = \int_E \phi^{1/2} f\,dx.$$

Since (32) defines $\mathbf{u}_h \in \mathbf{V}_h$ such that $\pi(d(\phi)\mathbf{v}_h) = \pi\mathbf{u}_h$ and (31) defines $p_h \in W_h$, we have that (41) holds. □

### 3.4 Solvability

**Lemma 3** *There exists a unique solution to the finite element method* (29)–(30).

*Proof* We recognize that $(\boldsymbol{\psi},\boldsymbol{\psi})_Q^{1/2}$ is a norm on $\mathbf{V}_h$ equivalent to $\|\boldsymbol{\psi}\|$ with bounds independent of $h$ [25]. Substituting $\boldsymbol{\psi}=\mathbf{v}_h-\mathbf{v}_{\mathrm{N}}\in\mathbf{V}_h$ and $w=q_h+\mathcal{P}_{W_h}[\hat{\phi}^{-1/2}\nabla\cdot(d(\phi)\mathbf{v}_h)]\in W_h$ into (29)–(30) and summing the two equations gives

$$\begin{aligned}
&(\mathbf{v}_h,\mathbf{v}_h)_Q+(q_h,q_h)+\big(\hat{\phi}^{-1/2}\nabla\cdot(d(\phi)\mathbf{v}_h),\mathcal{P}_{W_h}[\hat{\phi}^{-1/2}\nabla\cdot(d(\phi)\mathbf{v}_h)]\big)\\
&\quad+\langle\kappa^2\phi^{-1}(d(\phi))^2\mathbf{v}_h\cdot\boldsymbol{\nu},\mathbf{v}_h\cdot\boldsymbol{\nu}\rangle_{\mathrm{R}}\\
&=(d(\phi)\mathbf{g},\mathbf{v}_h-\mathbf{v}_{\mathrm{N}})-\langle g_{\mathrm{R}},\phi^{-1/2}d(\phi)\mathbf{v}_h\cdot\boldsymbol{\nu}\rangle_{\mathrm{R}}+(\mathbf{v}_h,\mathbf{v}_{\mathrm{N}})_Q-\big(q_h,\hat{\phi}^{-1/2}\nabla\cdot(d(\phi)\mathbf{v}_{\mathrm{N}})\big)\\
&\quad+(\hat{\phi}^{-1/2}\phi^{1/2}f,q_h+\mathcal{P}_{W_h}[\hat{\phi}^{-1/2}\nabla\cdot(d(\phi)\mathbf{v}_h)])-(q_h,\mathcal{P}_{W_h}[\hat{\phi}^{-1/2}\nabla\cdot(d(\phi)\mathbf{v}_h)]).
\end{aligned}$$

After introducing $\mathcal{P}_{W_h}$ in three places (term three on the left and terms four and five on the right), this then gives the bound (for any $\epsilon>0$ and where $C=C(\epsilon)$ is a generic positive constant)

$$\begin{aligned}
&(\mathbf{v}_h,\mathbf{v}_h)_Q+\|q_h\|^2+\|\mathcal{P}_{W_h}[\hat{\phi}^{-1/2}\nabla\cdot(d(\phi)\mathbf{v}_h)]\|^2+\|\kappa\phi^{-1/2}d(\phi)\mathbf{v}_h\cdot\boldsymbol{\nu}\|_{0,\Gamma_{\mathrm{R}}}^2\\
&\quad\le C\big\{\|\mathcal{P}_{W_h}[\hat{\phi}^{-1/2}\phi^{1/2}\,f]\|^2+\|d(\phi)\mathbf{g}\|^2+|\langle g_{\mathrm{R}},\phi^{-1/2}d(\phi)\mathbf{v}_h\cdot\boldsymbol{\nu}\rangle_{\mathrm{R}}|\\
&\qquad+\|\mathbf{v}_{\mathrm{N}}\|^2+\|\mathcal{P}_{W_h}[\hat{\phi}^{-1/2}\nabla\cdot(d(\phi)\mathbf{v}_{\mathrm{N}})]\|^2\big\}\\
&\qquad+\epsilon\big\{\|\mathbf{v}_h\|^2+\|q_h\|^2+\|\mathcal{P}_{W_h}[\hat{\phi}^{-1/2}\nabla\cdot(d(\phi)\mathbf{v}_h)]\|^2\big\}\\
&\qquad+\tfrac{1}{2}\big\{\|q_h\|^2+\|\mathcal{P}_{W_h}[\hat{\phi}^{-1/2}\nabla\cdot(d(\phi)\mathbf{v}_h)]\|^2\big\}.
\end{aligned}$$

Setting $\epsilon=1/4$, we obtain the estimate

$$\begin{aligned}
&\|\mathbf{v}_h\|^2+\|q_h\|^2+\|\mathcal{P}_{W_h}[\hat{\phi}^{-1/2}\nabla\cdot(d(\phi)\mathbf{v}_h)]\|^2+\|\kappa\phi^{-1/2}d(\phi)\mathbf{v}_h\cdot\boldsymbol{\nu}\|_{0,\Gamma_{\mathrm{R}}}^2 \qquad (43)\\
&\quad\le C\big\{\|\mathcal{P}_{W_h}[\hat{\phi}^{-1/2}\phi^{1/2}\,f]\|^2+\|d(\phi)\mathbf{g}\|^2+|\langle g_{\mathrm{R}},\phi^{-1/2}d(\phi)\mathbf{v}_h\cdot\boldsymbol{\nu}\rangle_{\mathrm{R}}|\\
&\qquad+\|\mathbf{v}_{\mathrm{N}}\|^2+\|\mathcal{P}_{W_h}[\hat{\phi}^{-1/2}\nabla\cdot(d(\phi)\mathbf{v}_{\mathrm{N}})]\|^2\big\}.
\end{aligned}$$

Uniqueness and, therefore, existence of the solution is established. □

### 3.5 Stability

We would like to establish stability of the solution by going further with the estimate (43). Unfortunately, we do not have a discrete version of the trace bound (22) involving $\hat{\phi}$ to estimate the term $|\langle g_{\mathrm{R}},\phi^{-1/2}d(\phi)\mathbf{v}_h\cdot\boldsymbol{\nu}\rangle_{\mathrm{R}}|$. By adding some hypotheses, we can obtain the following stability bound directly from (43):

$$\begin{aligned}
&\|\mathbf{v}_h\|+\|q_h\|+\|\mathcal{P}_{W_h}[\hat{\phi}^{-1/2}\nabla\cdot(d(\phi)\mathbf{v}_h)]\|+\|\kappa\phi^{-1/2}d(\phi)\mathbf{v}_h\cdot\boldsymbol{\nu}\|_{0,\Gamma_{\mathrm{R}}} \qquad (44)\\
&\quad\le C\big\{\|\mathcal{P}_{W_h}[\hat{\phi}^{-1/2}\phi^{1/2}\,f]\|+\|d(\phi)\mathbf{g}\|+\|g_{\mathrm{R}}\|_{0,\Gamma_{\mathrm{R}}}\\
&\qquad+\|\mathbf{v}_{\mathrm{N}}\|+\|\mathcal{P}_{W_h}[\hat{\phi}^{-1/2}\nabla\cdot(d(\phi)\mathbf{v}_{\mathrm{N}})]\|\big\}.
\end{aligned}$$

This holds when we use Neumann boundary conditions (so $\Gamma_{\mathrm{R}}=\emptyset$) and also when we have either homogeneous Robin conditions (so $g_{\mathrm{R}}=0$) or uniform Robin conditions, i.e., $\kappa\ge\kappa_*>0$ for some constant $\kappa_*$.

In the case of nonhomogeneous, nonuniform Robin boundary conditions, we can guarantee stability if we modify the method, in particular the treatment of $g_{\mathrm{R}}$ in (29). We base our modification on a discrete version of the definition of the normal trace (18). First, we require $\tilde{g}_{\mathrm{R}} \in H^1(\Omega)$, which is any extension of $g_{\mathrm{R}} \in H^{1/2}(\partial\Omega)$ to the interior of $\Omega$. Then

$$\begin{aligned}\langle g_{\mathrm{R}}, \phi^{-1/2} d(\phi)\mathbf{v}_h \cdot \boldsymbol{\nu}\rangle_{\mathrm{R}} &= \big(\tilde{g}_{\mathrm{R}}, \phi^{-1/2}\nabla\cdot(d(\phi)\mathbf{v}_h)\big) + \big(d(\phi)\nabla(\phi^{-1/2}\tilde{g}_{\mathrm{R}}), \mathbf{v}_h\big)\\ &\approx \big(\hat{\tilde{g}}_{\mathrm{R}}, \hat{\phi}^{-1/2}\nabla\cdot(d(\phi)\mathbf{v}_h)\big) + \big(d(\phi)\nabla(\phi^{-1/2}\tilde{g}_{\mathrm{R}}), \mathbf{v}_h\big).\end{aligned}$$

The modified method uses (30) combined with

$$\begin{aligned}&(\mathbf{v}_h, \boldsymbol{\psi})_Q - \big(q_h, \hat{\phi}^{-1/2}\nabla\cdot(d(\phi)\boldsymbol{\psi})\big) + \langle \kappa^2\phi^{-1}(d(\phi))^2\mathbf{v}_h\cdot\boldsymbol{\nu}, \boldsymbol{\psi}\cdot\boldsymbol{\nu}\rangle_{\mathrm{R}} \qquad (45)\\ &\quad = (d(\phi)\mathbf{g}, \boldsymbol{\psi}) - \big(\hat{\tilde{g}}_{\mathrm{R}}, \hat{\phi}^{-1/2}\nabla\cdot(d(\phi)\mathbf{v}_h)\big) - \big(d(\phi)\nabla(\phi^{-1/2}\tilde{g}_{\mathrm{R}}), \mathbf{v}_h\big)\ \forall\boldsymbol{\psi}\in\mathbf{V}_h.\end{aligned}$$

In this case, introduce $\mathcal{P}_{W_h}$ in the second term on the right to obtain the stability estimate (44) with the term $\|g_{\mathrm{R}}\|_{0,\Gamma_{\mathrm{R}}}$ replaced by $\|\tilde{g}_{\mathrm{R}}\|_1$.

**Lemma 4** *If $\Gamma_{\mathrm{R}} = \emptyset$, $g_{\mathrm{R}} = 0$, or $\kappa \geq \kappa_* > 0$ for some constant $\kappa_*$, then the solution to the finite element method* (29)–(30) *satisfies the stability bound* (44)*. Moreover, the modified mixed finite element method* (45) *and* (30) *satisfies the stability bound*

$$\begin{aligned}&\|\mathbf{v}_h\| + \|q_h\| + \|\mathcal{P}_{W_h}[\hat{\phi}^{-1/2}\nabla\cdot(d(\phi)\mathbf{v}_h)]\| + \|\kappa\phi^{-1/2}d(\phi)\mathbf{v}_h\cdot\boldsymbol{\nu}\|_{0,\Gamma_{\mathrm{R}}} \qquad (46)\\ &\quad\leq C\big\{\|\mathcal{P}_{W_h}[\hat{\phi}^{-1/2}\phi^{1/2}\,f]\| + \|d(\phi)\mathbf{g}\| + \|\tilde{g}_{\mathrm{R}}\|_1\\ &\qquad + \|\mathbf{v}_{\mathrm{N}}\| + \|\mathcal{P}_{W_h}[\hat{\phi}^{-1/2}\nabla\cdot(d(\phi)\mathbf{v}_{\mathrm{N}})]\|\big\}.\end{aligned}$$

## 4 Some numerical results

In this section we test the convergence of our proposed cell-centered finite difference scheme (29)–(30) using Dirichlet boundary conditions (but *without* using the stabilizing variant (45)). We fix the domain $\Omega = (-1,1)^n$ and use a uniform rectangular mesh of $m = 1/h$ elements in each coordinate direction. In some tests, we randomly perturb each mesh point $\mathbf{x} = (x_1, \ldots, x_n)$ not on the boundary. We choose $\xi_i$ randomly in the interval $[-h/4, h/4]$, $i = 1, \ldots, n$, and replace $\mathbf{x}$ by $\mathbf{x}+\xi$. This results in a rectangular mesh with unequal spacings. We implement the tests in terms of closed form and manufactured solutions. In the latter case, we give closed form expressions for $\phi$ and $p$ and from these we compute $f$ and Dirichlet boundary conditions (i.e., $\kappa = 0$). In all tests, $\mathbf{g} = 0$ and $d(\phi) = \phi$ (so $\mathbf{u} = \mathbf{v}$).

Since our method is cell-centered finite differences on a rectangular grid, we might expect that our method achieves $\mathcal{O}(h)$ convergence and even $\mathcal{O}(h^2)$ superconvergence for sufficiently regular solutions, since this is the case for nondegenerate elliptic problems [25]. Indeed, we see evidence of this assertion in the numerical results presented below.

We use discrete $L^2$-norms to measure the relative errors. For $p$ and $q$, we use the midpoint quadrature rule applied to the $L^2$-norm, which gives an approximation to $\|\hat{q} - q_h\|$ and $\|\hat{p} - p_h\|$. For $\mathbf{v}$, we use the trapezoidal rule applied to the $(L^2)^2$-norm, which is effectively like the norm $\|\pi\mathbf{v} - \mathbf{v}_h\|$. In both cases, these are norms for which superconvergence might be expected.

Our test cases are similar to those in [3], where a mixed finite element approximation to the system was proposed and analyzed.

### 4.1 A simple Euler equation in one dimension

Let $\Omega = (-1, 1)$ and for the parameter $\beta$, let

$$\phi(x) = \begin{cases} 0, & x < 0, \\ x^2, & x > 0. \end{cases} \quad \text{and} \quad f(x) = \begin{cases} 0, & x < 0, \\ x^{\beta+1}, & x > 0. \end{cases}$$

Assumption 1 holds for this porosity. As discussed in more detail in [3], our system of equations (5)–(6) reduces to the Euler equation

$$-x^2\, p'' - 4x\, p' + p = x^\beta, \quad 0 < x < 1, \tag{47}$$

for which the Euler exponents are

$$r_1 = \frac{-3 + \sqrt{13}}{2} \approx 0.3 > 0 \quad \text{and} \quad r_2 = \frac{-3 - \sqrt{13}}{2} \approx -3.3 < 0. \tag{48}$$

If we impose homogeneous Neumann boundary conditions and restrict $\beta \neq r_1, r_2$, the solution is

$$q(x) = x\, p(x) \quad \text{and} \quad p(x) = \begin{cases} 0, & -1 < x \le 0, \\ \dfrac{\beta x^{r_1} - r_1 x^\beta}{r_1(\beta - r_1)(\beta - r_2)}, & 0 < x < 1, \end{cases} \tag{49}$$

$$v(x) = u(x) = \begin{cases} 0, & -1 < x \le 0, \\ \dfrac{-\beta(x^{r_1+1} - x^{\beta+1})}{(\beta - r_1)(\beta - r_2)}, & 0 < x < 1, \end{cases} \tag{50}$$

wherein we arbitrarily set $p = 0$ for $x < 0$ since it is ill-defined there.

In terms of the potential singularity near $x = 0$, $q \sim u \sim |x|^{1.3} + |x|^{1+\beta}$ and $p \sim |x|^{0.3} + |x|^\beta$, and so for any $\epsilon > 0$,

$$q, u \in H^{\min(1.8, 3/2+\beta)-\epsilon} \quad \text{and} \quad p \in H^{\min(0.8, 1/2+\beta)-\epsilon}.$$

We consider four values of $\beta$, $\beta = 1/2$, $-1/2$, $-1$, and $-3/2$. The numerical results are presented in Table 1. Based on the regularity of the solution, if the solution exhibited superconvergence, we would expect the order of convergence for $q$ and $u$ to be $\mathcal{O}(h^{1.8})$ for $\beta = 1/2$, $\mathcal{O}(h^1)$ for $\beta = -1/2$, $\mathcal{O}(h^{1/2})$ for $\beta = -1$, and no convergence for $\beta = -3/2$. These rates are seen, approximately, in the numerical results. Moreover, the order of convergence for $p$ should be $\mathcal{O}(h^{0.8})$ for $\beta = 1/2$ and no convergence for the other values of $\beta$, which we also see approximately. The results show less error (even on coarser grids) and better convergence than those in [3] for the mixed finite element method.

We remark that the convergence rate is slightly better if instead of using (37), we simply set $b_E = (f, w_E)$. This, of course, would lead to a loss of strict local mass conservation.

If we perturb the computational meshes, we continue to see similar convergence and superconvergence results. We show in Fig. 1 the relative error for $q$, $u$, and $p$ on a log scale versus $m$ on a log scale. When $\beta = 1/2$, the errors in $q$ and $u$ show a clear rate of superconvergence $\mathcal{O}(h^{1.8})$. The error in $p$ bounces around due to the randomness of the perturbation, but it appears to converge at the rate $\mathcal{O}(h^{0.8})$. When $\beta = -1/2$ and $-1$, $q$ and $u$ appear to convergence at the expected rates $\mathcal{O}(h^1)$ and $\mathcal{O}(h^{0.5})$, respectively, although the errors bounce around a bit. There is no apparent convergence for $p$ when $\beta = -1/2$ and $-1$.

**Table 1** Euler's equation. Shown are the relative discrete $L^2$-norm errors of $q$, $p$, and $\mathbf{u}$ for various number of elements $m \times m$ and for four values of $\beta$. The convergence rate corresponds to a superconvergent approximation, restricted by the regularity of the true solution.

| | | scaled pressure $q$ | | pressure $p$ | | velocity $u$ | |
|---|---|---|---|---|---|---|---|
| $\beta$ | $m$ | error | rate | err | rate | err | rate |
| 0.5 | 32 | 0.002043 | — | 0.006756 | — | 0.007438 | — |
| | 64 | 0.000642 | 1.669 | 0.004341 | 0.638 | 0.002387 | 1.640 |
| | 128 | 0.000199 | 1.691 | 0.002724 | 0.672 | 0.000754 | 1.663 |
| | 256 | 0.000061 | 1.709 | 0.001681 | 0.697 | 0.000235 | 1.681 |
| | 512 | 0.000018 | 1.723 | 0.001024 | 0.716 | 0.000073 | 1.695 |
| −0.5 | 32 | 0.001913 | — | 0.040343 | — | 0.013276 | — |
| | 64 | 0.000802 | 1.254 | 0.039971 | 0.013 | 0.006749 | 0.976 |
| | 128 | 0.000358 | 1.166 | 0.039289 | 0.025 | 0.003426 | 0.978 |
| | 256 | 0.000167 | 1.101 | 0.038474 | 0.030 | 0.001731 | 0.985 |
| | 512 | 0.000080 | 1.060 | 0.037617 | 0.033 | 0.000872 | 0.990 |
| −1.0 | 32 | 0.006379 | — | 0.155115 | — | 0.015402 | — |
| | 64 | 0.004849 | 0.396 | 0.164987 | -0.089 | 0.010550 | 0.546 |
| | 128 | 0.003526 | 0.460 | 0.170768 | -0.050 | 0.007338 | 0.524 |
| | 256 | 0.002521 | 0.484 | 0.173955 | -0.027 | 0.005142 | 0.513 |
| | 512 | 0.001790 | 0.494 | 0.175645 | -0.014 | 0.003618 | 0.507 |
| −1.5 | 32 | 0.060245 | — | 0.273779 | — | 0.004816 | — |
| | 64 | 0.059596 | 0.016 | 0.278083 | -0.023 | 0.003470 | 0.473 |
| | 128 | 0.058620 | 0.024 | 0.279416 | -0.007 | 0.002856 | 0.281 |
| | 256 | 0.057593 | 0.026 | 0.279819 | -0.002 | 0.002507 | 0.188 |
| | 512 | 0.056590 | 0.025 | 0.279939 | -0.001 | 0.002281 | 0.137 |

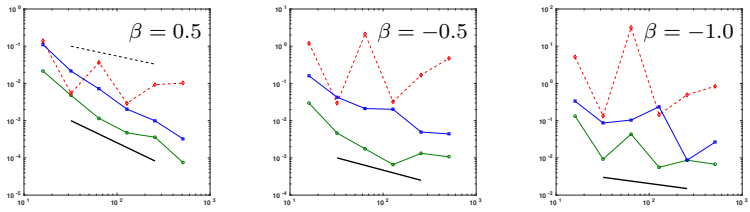


**Fig. 1** Euler's equation on perturbed meshes. Shown is the log-log relative error versus $m$ for the scaled pressure $q$ (circles), velocity $u$ (squares), and pressure $p$ (diamonds with dashed line). Also shown is the expected convergence rate for $q$ and $u$ (solid line) and $p$ (dashed line). These rates are 1.8, 1.0, and 0.5 for $q$ and $u$ when $\beta = 0.5$, $-0.5$, and $-1.0$, respectively, and only 0.8 for the $p$ when $\beta = 0.5$.

### 4.2 A smooth solution test in two-dimensions

For the next series of tests, we assume that $p = \cos(6xy^2)$ is smooth and that $\phi$ is given by

$$\phi = \begin{cases} 0 & \text{if } x \le -3/4 \text{ or } y \le -3/4, \\ (x+3/4)^\alpha (y+3/4)^{2\alpha} & \text{otherwise.} \end{cases} \tag{51}$$

We note that $\phi^{-1/2}\nabla\phi = \alpha\big((x+3/4)^{\alpha/2-1}(y+3/4)^\alpha, 2(x+3/4)^{\alpha/2}(y+3/4)^{\alpha-1}\big)$ is in $\big(L^\infty((-1,1)^2)\big)^2$ if and only if $\alpha \ge 2$. Nevertheless, we consider the four values $\alpha = 2$, 1, 1/4, and 1/8. The singularity in $x$ along $x = -3/4$ implies that for any $\epsilon > 0$,

$$q \in H^{(\alpha+1)/2-\epsilon} \quad \text{and} \quad \mathbf{u} \in \big(H^{\alpha+1/2-\epsilon}\big)^2.$$

**Table 2** Smooth $p$ two-dimensional test. Shown are the relative discrete $L^2$-norm errors of $q$, $p$, and $\mathbf{u}$ for various number of elements $m \times m$ and for four values of $\alpha$ defining $\phi$. The convergence rate is better than expected for low values of $\alpha$.

| | | scaled pressure $q$ | | pressure $p$ | | velocity $\mathbf{u}$ | |
|---|---|---|---|---|---|---|---|
| $\alpha$ | $m$ | error | rate | err | rate | err | rate |
| 2 | 32 | 0.012878 | — | 0.020996 | — | 0.029391 | — |
| | 64 | 0.003260 | 1.982 | 0.007574 | 1.471 | 0.009392 | 1.646 |
| | 128 | 0.000825 | 1.983 | 0.002655 | 1.512 | 0.002791 | 1.751 |
| | 256 | 0.000209 | 1.979 | 0.000924 | 1.523 | 0.000795 | 1.811 |
| | 512 | 0.000054 | 1.966 | 0.000322 | 1.521 | 0.000221 | 1.849 |
| 1 | 32 | 0.007507 | — | 0.008594 | — | 0.023786 | — |
| | 64 | 0.001929 | 1.961 | 0.002941 | 1.547 | 0.007442 | 1.676 |
| | 128 | 0.000493 | 1.966 | 0.001001 | 1.555 | 0.002182 | 1.770 |
| | 256 | 0.000127 | 1.955 | 0.000343 | 1.545 | 0.000616 | 1.824 |
| | 512 | 0.000034 | 1.924 | 0.000119 | 1.533 | 0.000170 | 1.858 |
| 0.25 | 32 | 0.007443 | — | 0.009351 | — | 0.019810 | — |
| | 64 | 0.004953 | 0.588 | 0.006521 | 0.520 | 0.008355 | 1.246 |
| | 128 | 0.003549 | 0.481 | 0.004687 | 0.476 | 0.004913 | 0.766 |
| | 256 | 0.002528 | 0.490 | 0.003348 | 0.485 | 0.003429 | 0.519 |
| | 512 | 0.001788 | 0.500 | 0.002380 | 0.493 | 0.002469 | 0.474 |
| 0.125 | 32 | 0.066864 | — | 0.082809 | — | 0.048566 | — |
| | 64 | 0.053265 | 0.328 | 0.065477 | 0.339 | 0.038811 | 0.323 |
| | 128 | 0.042347 | 0.331 | 0.051784 | 0.338 | 0.032259 | 0.267 |
| | 256 | 0.033806 | 0.325 | 0.041165 | 0.331 | 0.026911 | 0.262 |
| | 512 | 0.027147 | 0.317 | 0.032935 | 0.322 | 0.022434 | 0.263 |

The results given in Table 2 show good convergence for this problem for $\alpha = 2$ and 1, and some degradation for the smaller values of $\alpha$. Perhaps Assumption 1 is stronger than needed for convergence. The results suggest that it may be enough that $\phi^{-1/2}\nabla\phi \in \left(L^2((-1,1)^2)\right)^2$, which is true here if and only if $\alpha > 1$. Again, the results show some superconvergence and less error on coarser grids than those in [3] for the mixed finite element method.

The solution $p$ and $q$ are shown in Figure 2. Although $p$ is smooth, we show $p = 0$ in the one-phase region, since it is ill-defined there. In this way, one can clearly see that in fact $p$ is not smooth on the boundary between the one and two phase regions $\mathcal{B} = \{x = -3/4, y \geq -3/4\} \cup \{x \geq -3/4, y = -3/4\}$. The scaled pressure $q$ is, however, well behaved for $\alpha = 2$ and degenerates near $\mathcal{B}$ as $\alpha$ decreases (i.e., as $\phi^{1/2}\nabla\phi$ loses its regularity).

When the number of grid cells $m$ is even, the one-phase/two-phase transition $\mathcal{B}$ lies on a grid line. If we take an odd number of elements, we will avoid this. Results are shown in Table 3. When $\alpha = 2$, we see similar errors and rates of convergence as for the case of $\mathcal{B}$ being resolved by the grid in Table 2. However, the errors are worse for the more challenging case of $\alpha = 1/4$, although the convergence rates seem to settle to about the same values.

When we use perturbed rectangular meshes, the boundary $\mathcal{B}$ is not resolved. We see similar convergence behavior as for uniform meshes, as can be seen in Fig. 3.

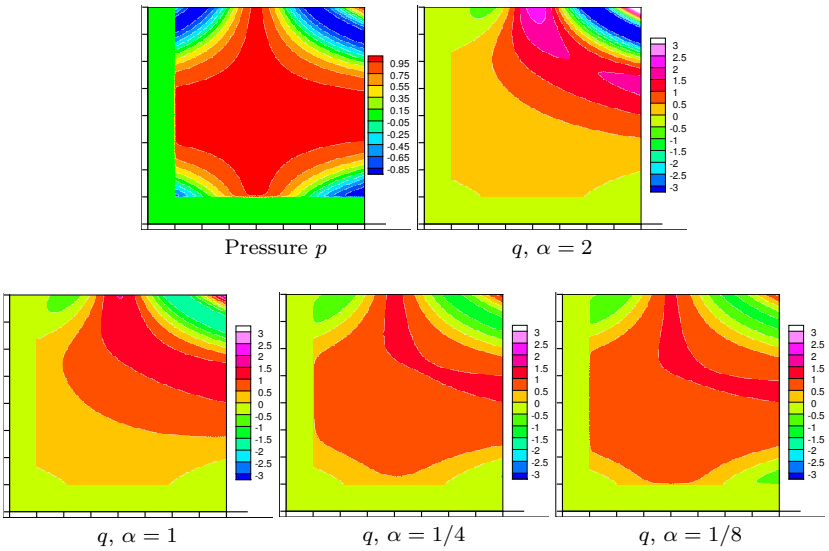


**Fig. 2** Smooth $p$ two-dimensional test. Shown are the pressure $p$ and scaled pressure $q$ for four values of $\alpha$ defining $\phi$. The pressure is smooth, except on the boundary of the support of $\phi$ (i.e., $x = -3/4$ or $y = -3/4$). The scaled pressure becomes less regular as $\alpha$ decreases near the boundary.

**Table 3** Smooth $p$ two-dimensional test. Shown are the relative discrete $L^2$-norm errors of $q$, $p$, and $\mathbf{u}$ for various odd numbers of elements $m \times m$ and for $\alpha = 2$ and 0.25 defining $\phi$. The convergence is similar to the case of grids that resolve the boundary between the one and two phase regions when $\alpha = 2$, but not for $\alpha = 1/4$.

| | | scaled pressure $q$ | | pressure $p$ | | velocity $\mathbf{u}$ | |
|---|---|---|---|---|---|---|---|
| $\alpha$ | $m$ | error | rate | err | rate | err | rate |
| 2 | 33 | 0.012137 | — | 0.021447 | — | 0.028001 | — |
| | 65 | 0.003171 | 1.980 | 0.007832 | 1.486 | 0.009146 | 1.651 |
| | 129 | 0.000817 | 1.979 | 0.002769 | 1.517 | 0.002753 | 1.752 |
| | 257 | 0.000210 | 1.971 | 0.000969 | 1.523 | 0.000790 | 1.811 |
| | 513 | 0.000055 | 1.938 | 0.000339 | 1.520 | 0.000220 | 1.850 |
| 0.25 | 33 | 0.031315 | — | 0.047229 | — | 0.039155 | — |
| | 65 | 0.020907 | 0.596 | 0.029933 | 0.673 | 0.024967 | 0.664 |
| | 129 | 0.014105 | 0.574 | 0.019492 | 0.626 | 0.017147 | 0.548 |
| | 257 | 0.009588 | 0.560 | 0.012969 | 0.591 | 0.012062 | 0.510 |
| | 513 | 0.006566 | 0.548 | 0.008778 | 0.565 | 0.008545 | 0.499 |

### 4.3 A nonsmooth solution test in two-dimensions

For the final series of tests, we take $\phi$ as given by (51) with $\alpha = 2$, and we impose the nonsmooth pressure solution

$$p = y(y - 3x)(x + 3/4)^{\beta}, \quad \beta = -1/4 \text{ or } -3/4. \tag{52}$$

This pressure and the scaled pressure $q = \phi^{1/2}p$ are shown in Fig. 4, where one can see clearly the degeneracy in $p$ near $x = -3/4$ and that $q$ is better behaved. In the case $\beta = -1/4$, $q$ and $\mathbf{u}$ lie in $H^{1.25-\epsilon}$ and are relatively smooth, whereas when $\beta = -3/4$, $q$ and $\mathbf{u}$ lie only in $H^{0.75-\epsilon}$, for any $\epsilon > 0$.

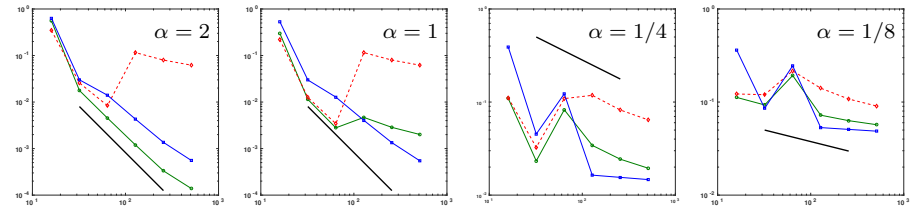


**Fig. 3** Smooth $p$ two-dimensional test on perturbed meshes. Shown is the log-log relative error versus $m$ for the scaled pressure $q$ (circles), velocity $u$ (squares), and pressure $p$ (diamonds with dashed line). Also shown is the assumed convergence rate for $q$ and $u$ (solid line), based on the uniform mesh results. These rates are 2, 2, 0.5, and 0.25 when $\alpha = 2$, 1, 1/4, and 1/8.

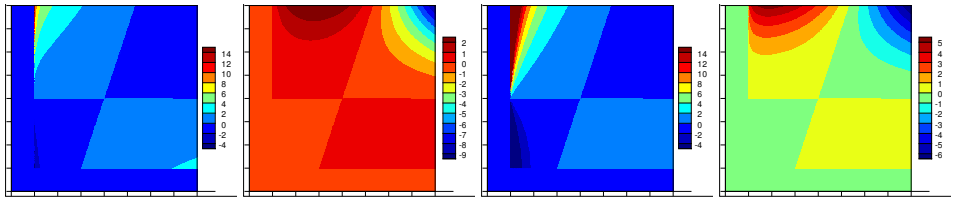

$p$, $\beta = -1/4$ $q$, $\beta = -1/4$ $p$, $\beta = -3/4$ $q$, $\beta = -3/4$

**Fig. 4** Nonsmooth $p$ two-dimensional test. Shown are the pressure $p$ and scaled pressure $q$ for two values of $\beta$ in (52). The pressures is smooth, except on the boundary of the support of $\phi$ (i.e., $x = -3/4$ or $y = -3/4$). The two pressures become less regular near the boundary as $\beta$ decreases.

**Table 4** Nonsmooth $p$ two-dimensional test. Shown are the relative discrete $L^2$-norm errors of $q$, $p$, and $\mathbf{u}$ for various odd numbers of elements $m \times m$ and for $\beta = -1/4$ and $-3/4$ defining $p$ in (52).

| | | scaled pressure $q$ | | pressure $p$ | | velocity $\mathbf{u}$ | |
|---|---|---|---|---|---|---|---|
| $\beta$ | $m$ | error | rate | err | rate | err | rate |
| $-1/4$ | 33 | 0.005050 | — | 0.045199 | — | 0.002885 | — |
| | 65 | 0.002193 | 1.231 | 0.034160 | 0.413 | 0.000786 | 1.918 |
| | 129 | 0.000944 | 1.230 | 0.027326 | 0.326 | 0.000211 | 1.919 |
| | 257 | 0.000402 | 1.239 | 0.022448 | 0.285 | 0.000056 | 1.925 |
| | 513 | 0.000171 | 1.237 | 0.018661 | 0.267 | 0.000015 | 1.906 |
| $-3/4$ | 33 | 0.004155 | — | 0.193534 | — | 0.004991 | — |
| | 65 | 0.002554 | 0.718 | 0.184637 | 0.069 | 0.002113 | 1.268 |
| | 129 | 0.001608 | 0.675 | 0.179129 | 0.044 | 0.000935 | 1.190 |
| | 257 | 0.000991 | 0.702 | 0.175644 | 0.029 | 0.000432 | 1.120 |
| | 513 | 0.000601 | 0.724 | 0.173380 | 0.019 | 0.000210 | 1.044 |

We use grids that do *not* resolve the interface between the one and two-phase regions. The discrete errors and convergence rates are shown in Table 4. The scaled pressure converges as expected, and the velocity seems to be converging a bit better than expected. The pressure barely converges at all. Again in this test case we see results that show some superconvergence and less error on coarser grids than those in [3] for the mixed finite element method.

As can be seen in Fig. 5, perturbed rectangular meshes give similar convergence behavior as for uniform meshes, although the convergence is not nearly as consistent.

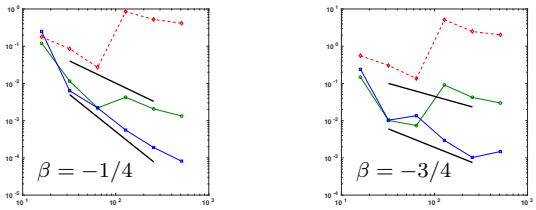


**Fig. 5** Nonsmooth $p$ two-dimensional test on perturbed meshes. Shown is the log-log relative error versus $m$ for the scaled pressure $q$ (circles), velocity $u$ (squares), and pressure $p$ (diamonds with dashed line). Also shown is the assumed convergence rate for $q$ and $u$ (solid lines), based on the uniform mesh results. These rates are 2 and 1 for $u$ and 1.2 and 0.7 for $q$ when $\beta = -1/4$ and $-3/4$, respectively.

## 5 Conclusions

We developed an easy to implement, locally mass conservative, and stable cell-centered finite difference method (29)–(30) for the degenerate problem (5)–(8). The method is an approximation of the scaled variational formulation (24)–(25), which is well-posed provided Assumption 1 holds. This assumption allows $\phi$ to degenerate on a set of positive measure. A straightforward finite element method based on this formulation was given in [3]. Here, we further approximated the problem by applying trapezoidal quadrature to one term (the velocity mass-matrix (34)), approximated the divergence operator on an element of the mesh $E$ as

$$\phi^{-1/2}\nabla(d(\phi)\mathbf{v}) \approx {\phi_E}^{-1/2}\nabla(d(\phi)\mathbf{v}), \tag{53}$$

where $\phi_E$ is the average of $\phi$ on $E$, and we modified the source term $f \approx \hat{\phi}^{-1/2}\phi^{1/2}f$ for local mass conservation.

The numerical tests in one and two space dimensions demonstrated that the method can achieve superconvergent rates of convergence with respect to the regularity of the velocity and scaled pressure. Convergence of the true pressure was generally relatively poor. In some tests, optimal convergence rates were observed even when a weaker condition than Assumption 1 held, namely, $\phi^{-1/2}\nabla\phi \in L^2$ versus $L^\infty$. In some of the tests, the meshes did not match the boundary of the one-phase region, and we observed no degradation of results from cases with meshes that match this boundary.

Unlike the mixed finite element method in [3], our new cell-centered finite difference method is locally conservative and easy to implement. Moreover, the numerical tests suggest that the new method achieves better convergence rates (superconvergence) and less error on coarse grids than the former method.

## Acknowledgment

The authors thank Professor Marc A. Hesse for many insightful conversations on the mantle dynamics system.

## References


1. E. Aharonov, J. A. Whitehead, P. B. Kelemen, and M. Spiegelman, *Channeling instability of upwelling melt in the mantle*, J. Geophysical Research, 100 (1995), pp. 20433–20450.
2. T. Arbogast, M. A. Hesse, and A. L. Taicher, *Mixed methods for two-phase Darcy-Stokes mixtures of partially melted materials with regions of zero porosity*, SIAM J. Sci. Comput., 39 (2017), pp. B375–B402. DOI 10.1137/16M1091095.
3. T. Arbogast and A. L. Taicher, *A linear degenerate elliptic equation arising from two-phase mixtures*, SIAM J. Numer. Anal., 54 (2016), pp. 3105–3122. DOI 10.1137/16M1067846.
4. T. Arbogast, M. F. Wheeler, and I. Yotov, *Mixed finite elements for elliptic problems with tensor coefficients as cell-centered finite differences*, SIAM J. Numer. Anal., 34 (1997), pp. 828–852.
5. D. Arroyo, A. Bespalov, and N. Heuer, *On the finite element method for elliptic problems with degenerate and singular coefficients*, Math. Comp., 76 (2007), pp. 509–537.
6. A. Aschwanden, E. Bueler, C. Khroulev, and H. Blatter, *An enthalpy formulation for glaciers and ice sheets*, J. Glaciology, 58 (2012), pp. 441–457.
7. J. Bear, *Dynamics of Fluids in Porous Media*, Dover, New York, 1972.
8. J. Bear and A. H.-D. Cheng, *Modeling Groundwater Flow and Contaminant Transport*, Springer, New York, 2010.
9. S. Bidwell, M. E. Hassell, and C. R. Westphal, *A weighted least squares finite element method for elliptic problems with degenerate and singular coefficients*, Math. Comp., 82 (2013), pp. 673–688.
10. F. Brezzi and M. Fortin, *Mixed and hybrid finite element methods*, Springer-Verlag, New York, 1991.
11. Z. Chen, G. Huan, and Y. Ma, *Computational Methods for Multiphase Flows in Porous Media*, vol. 2 of Computational Science and Engineering Series, SIAM, Philadelphia, 2006.
12. K. Eriksson and V. Thomée, *Galerkin methods for singular boundary value problems in one space dimension*, Math. Comp., 42 (1984), pp. 345–367.
13. A. C. Fowler, *On the transport of moisture in polythermal glaciers*, Geophys. Astrophys. Fluid Dynamics, 28 (1984), pp. 99–140.
14. M. A. Hesse, A. R. Schiemenz, Y. Liang, and E. M. Parmentier, *Compaction-dissolution waves in an upwelling mantle column*, Geophysical J. Int., 187 (2011), pp. 1057–1075.
15. I. J. Hewitt and A. C. Fowler, *Partial melting in an upwelling mantle column*, Proc. R. Soc. A, 464 (2008), pp. 2467–2491.
16. R. F. Katz, *Magma dynamics with the enthalpy method: Benchmark solutions and magmatic focusing at mid-ocean ridges*, J. Petrology, 49 (2008), pp. 2099–2121.
17. L. W. Lake, *Enhanced Oil Recovery*, Prentice Hall, Englewood Cliffs, New Jersey, 1989.
18. H. Li, *A-priori analysis and the finite element method for a class of degenerate elliptic equations*, Math. Comp., 78 (2009), pp. 713–737.
19. D. Marini and P. Pietra, *Mixed finite element approximation of a degenerate elliptic problem*, Numer. Math., 71 (1995), pp. 225–236.
20. D. McKenzie, *The generation and compaction of partially molten rock*, J. Petrology, 25 (1984), pp. 713–765.
21. R. A. Raviart and J. M. Thomas, *A mixed finite element method for 2nd order elliptic problems*, in Mathematical Aspects of Finite Element Methods, I. Galligani and E. Magenes, eds., no. 606 in Lecture Notes in Math., Springer-Verlag, New York, 1977, pp. 292–315.
22. J. E. Roberts and J.-M. Thomas, *Mixed and hybrid methods*, in Handbook of Numerical Analysis, P. G. Ciarlet and J. L. Lions, eds., vol. 2, North-Holland, Amsterdam, 1991, pp. 523–639.
23. T. F. Russell and M. F. Wheeler, *Finite element and finite difference methods for continuous flows in porous media*, in The Mathematics of Reservoir Simulation, R. E. Ewing, ed., no. 1 in Frontiers in Applied Mathematics, Society for Industrial and Applied Mathematics, Philadelphia, 1983, pp. 35–106, Chapter II.
24. C. J. van der Veen, *Fundamentals of Glacier Dynamics*, CRC Press, second ed., 2013.
25. A. Weiser and M. F. Wheeler, *On convergence of block-centered finite-differences for elliptic problems*, SIAM. J. Numer. Anal., 25 (1988), pp. 351–375.
26. W. Zhu, G. Gaetani, F. Fusseis, L. Montesi, and F. D. Carlo, *Microtomography of partiallty molten rocks: three dimensional melt distribution in mantle peridotite*, Science, 332 (2011), pp. 88–91.